

Docking-based CoMFA and CoMSIA studies of non-nucleoside reverse transcriptase inhibitors of the pyridinone derivative type

J.L. Medina-Franco*, S. Rodríguez-Morales, C. Juárez-Gordiano, A. Hernández-Campos & R. Castillo**

Departamento de Farmacia, Facultad de Química, UNAM, CU, DF 04510, Mexico

Received 19 April 2004; accepted in revised form 26 July 2004

Key words: AutoDock, CoMFA, CoMSIA, 3D-QSAR, docking, HIV-1, non-nucleoside inhibitors, reverse transcriptase

Summary

Comparative molecular field analysis (CoMFA) and comparative molecular similarity indices analysis (CoMSIA) were performed on a set of pyridinone derivatives. A molecular alignment obtained by docking of compounds into the non-nucleoside reverse transcriptase inhibitor binding site of HIV-1 was used. Good correlations between the calculated binding free energies and experimental inhibitory activities suggest that the binding conformations of these inhibitors are reasonable. Robust and predictive 3D-QSAR models were obtained with q^2 values of 0.706 and 0.723 for CoMFA and CoMSIA, respectively. The models were validated by an external test set obtaining r^2_{pred} values of 0.720 and 0.750 for CoMFA and CoMSIA, respectively. The CoMFA, CoMSIA and docking results help to understand the type of interactions that occur between pyridinone derivatives with the non-nucleoside reverse transcriptase inhibitor binding pocket, and explain the viral resistance to pyridinone derivatives upon mutation of amino acids Tyr181 and Tyr188. The results obtained provide information for a better understanding of the drug resistant mechanisms. The 3D-QSAR models derived will be used to guide the design of pyridinone derivatives active against mutant strains of reverse transcriptase.

Abbreviations: AIDS, acquired immunodeficiency syndrome; CoMFA, comparative molecular field analysis; CoMSIA, comparative molecular similarity indices analysis; HIV, human immunodeficiency virus; NNRTIs, non-nucleoside reverse transcriptase inhibitors; PLS, partial least squares; QSAR, quantitative structure-activity relationships; RT, reverse transcriptase.

Introduction

The reverse transcriptase (RT) of human immunodeficiency virus type 1 (HIV-1) is an attractive target to treat the acquired immune deficiency syndrome (AIDS) for which no absolute successful chemotherapy is available to date [1]. RT inhibitors are classified in nucleoside and non-nucleoside depending on their mechanism of action. One advantage of the second group is that they lack the toxic effects associated

with the nucleosides. To date, three non-nucleoside RT inhibitors (NNRTIs) have been approved for clinical use named nevirapine (VIRAMUNE®) (Figure 1), delavirdine (RESCRIPTOR®) and efavirenz (SUSTIVA®) [1]. However, all these and other approved drugs induce drug resistant variants of HIV-1 [2].

Several crystal structures of HIV-1 RT in the apo form [3] and complexed with different NNRTIs have been published [4]. The non-nucleoside inhibitor binding pocket of HIV-1 RT is formed by the amino acids Pro95, Leu100, Lys101, Lys103, Val106, Val179, Tyr181, Tyr188, Gly190, Phe227, Trp229, Leu234,

*This work is part of the Ph.D. thesis of J.L. Medina-Franco.

**To whom correspondence should be addressed. Fax: +52-5622-5329; E-mail: rafaelc@servidor.unam.mx

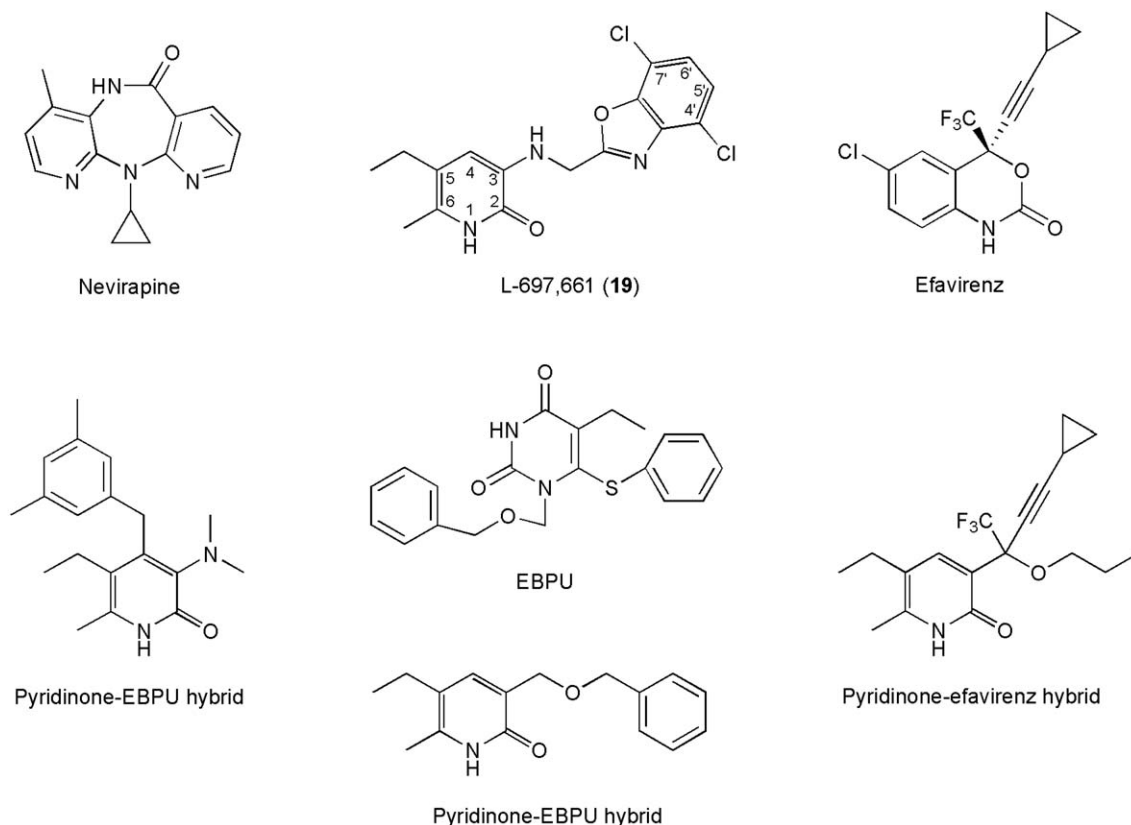


Figure 1. Chemical structures of nevirapine, L-697,661, efavirenz, EBPU, pyridinone-EBPU and pyridinone-efavirenz.

His235, Pro236 and Tyr318 of the p66 subunit and Glu138 of the p51 subunit. Crystal structures of RT-NNRTIs complexes reveal that some amino acids of the binding pocket adopt different conformations when bound to different inhibitors, leading to distinct pocket volumes [4b, 4f, 4i]. Despite these variations, several NNRTIs have a common binding mode with a butterfly-like conformation [4].

Pyridinone derivatives [5] are a class of NNRTIs [2]. No crystal structures of HIV-1 RT in complex with pyridinone derivatives have been published. However, several two-dimensional quantitative structure-activity relationship analyses (2D-QSAR) [6, 7] have been performed for pyridinone analogues suggesting a hydrophobic character of their binding pocket. Furthermore, from kinetic [5] and analysis of resistance mutations [8] it was concluded that this type of inhibitors should be binding in the same pocket as other NNRTIs. Extensive structure-activity relationships (SAR) studies have been conducted for these compounds leading to potent RT inhibitors [9–12]. Compound L-697,661 (**19**) (Figure 1) was subjected to clinical studies

showing good activity in patients, but rapid resistant strains of the virus emerged [13, 14]. The Tyr181Cys, Tyr188Cys and Lys103Asn mutations are responsible for the emergence of resistant virus not only for **19** but also for other pyridinone derivatives [14–16]. The Tyr181Cys mutation is the most important. Interesting to note, hybrid pyridinone-NNRTIs molecules have shown inhibitory activity against wild type and some mutant strains of RT (Figure 1) [17–20].

Several studies employing different QSAR methodologies have been performed on NNRTIs. Examples of recent works can be found in Refs. 21 and 22. Three-dimensional quantitative structure-activity relationship (3D-QSAR) methods such as comparative molecular field analysis (CoMFA) [23] and comparative molecular similarity indices analysis (CoMSIA) [24] have been successfully applied in many instances to guide the design of new active molecules [25]. For several NNRTIs, 3D-QSAR studies have helped to identify the type of interactions between the inhibitors and RT [26–30]. However, these methodologies have not been applied to pyridinone derivatives. Also,

molecular docking has been applied to understand the binding mode of NNRTIs and design novel molecules [26, 30–33]. We recently performed a docking study of potent pyridinone RT inhibitors and pyridinone hybrid molecules into the NNRTI binding pocket, proposing a binding mode for these molecules [34].

We now report in this paper CoMFA and CoMSIA studies of pyridinone derivatives based on the docking positions determined by the automated docking program AutoDock. The combination of ligand-based with structure-based drug design approaches is an attractive strategy for pyridinone derivatives for which the binding site is known but the binding mode has not been determined experimentally. Successful studies applying a combination of ligand-based approaches with structure-based approaches have been reported recently [30, 35–38]. The purposes of this work are (a) to investigate the type of interactions that occur between the pyridinone derivatives and the NNRTI binding pocket; and (b) to identify the structural requirements for HIV-1 RT inhibitory activity of pyridinone derivatives. 3D-QSAR results will further validate the docking models.

Computational methods

Data set and biological data

A set of 40 pyridinone derivatives taken from literature [11, 12] was divided into a training set of 29 compounds and a test set of 11 compounds, sampling from various ranges of logarithmic unit of activities. The chemical structures of the training and test sets are depicted in Tables 1 and 2, respectively. The experimental RT inhibitory activities were estimated under the same experimental conditions. Activities were converted into the corresponding $-\log IC_{50}$ values, where IC_{50} is the effective concentration of compound required to achieve 50% of inhibition of RT. The observed biological activities are given in Tables 1 and 2.

Molecular docking

Automated docking was used to locate the appropriate binding orientations and conformations of pyridinone derivatives into the NNRTI binding pocket. The powerful genetic algorithm method implemented in the program AutoDock 3.0 [39] was employed. RT in complex with nevirapine [4a], the structure with the highest resolution available, was used. Furthermore,

in a previous docking study of pyridinone derivatives into several NNRTI binding pocket geometries it was concluded that the binding pocket of nevirapine is a good model to study the binding mode of pyridinone analogues [34]. The structure was retrieved from the RCSB Protein Data Base (PDB entry 1VRT) [40].

The structures of pyridinone derivatives and RT were prepared using Sybyl 6.8 [41]. Molecular structures of pyridinone derivatives were built using the SKETCH option in Sybyl. Geometry optimizations were performed using the Tripos force field [42] with a distance-dependent dielectric and the Powell conjugate gradient algorithm. Gasteiger-Hückel charges [43] were used.

All water molecules and magnesium ions were removed from the original Protein Data Bank file. Polar hydrogen atoms were added and Kollman charges [44], atomic solvation parameters and fragmental volumes were assigned to the protein using AutoDock Tools (ADT). For validation of the docking protocol, nevirapine coordinates in the crystal complex were removed and the bond orders were checked. For docking calculations, Gasteiger partial charges [45] were assigned to the pyridinone derivatives and nevirapine, and non-polar hydrogen atoms were merged. All torsions were allowed to rotate during docking.

The auxiliary program AutoGrid generated the grid maps. Each grid was centered at the crystal structure of the corresponding NNRTI. The grid dimensions were $23 \times 23 \times 23 \text{ \AA}^3$ with points separated by 0.375 \AA . Lennard-Jones parameters 12-10 and 12-6, supplied with the program, were used for modeling H-bonds and van der Waals interactions, respectively. The distance-dependent dielectric permittivity of Mehler and Solmajer [46] was used for calculation of the electrostatic grid maps. For all ligands, random starting positions, random orientations and torsions were used. The translation, quaternion and torsion steps were taken from default values in AutoDock. The Lamarckian genetic algorithm and the pseudo-Solis and Wets methods were applied for minimization using default parameters. The number of docking runs was 100. The population in the genetic algorithm was 50, the energy evaluations were 250 000 and the maximum number of iterations 27 000.

After docking, the 100 solutions were clustered into groups with RMS deviations lower than 1.0 \AA . The clusters were ranked by the lowest energy representative of each cluster.

The complexes of pyridinone derivatives with HIV-1 RT resulting from molecular docking were further

Table 1. Structures, HIV-1 RT inhibitory activity and AutoDock binding free energies of compounds in the training set.

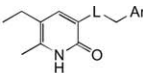
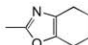
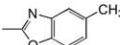
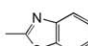
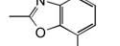
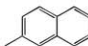
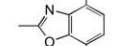
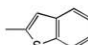
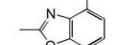
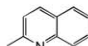
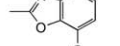
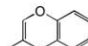
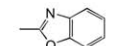
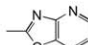
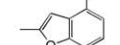
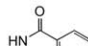

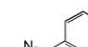
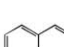
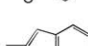
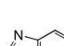

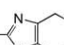
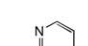
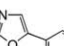
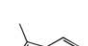
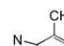
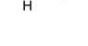
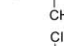
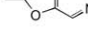
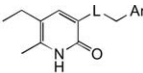
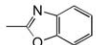
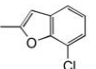
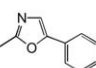
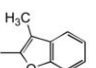
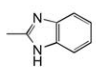
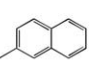
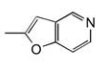
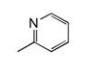
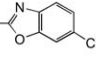
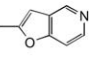
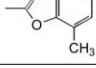
<div>  </div>									
Comp.	L	Ar	-LogIC ₅₀	ΔG (kcal/mol)	Comp.	L	Ar	-LogIC ₅₀	ΔG (kcal/mol)
1	NH		6.55	-9.34	16	NH		5.90	-9.02
2	NH		6.46	-9.25	17	NH		6.59	-9.65
3	NH		6.34	-9.53	18	NH		7.7	-10.01
4	NH		6.30	-9.24	19	NH		7.72	-9.83
5	NH		6.28	-9.56	20	NH		6.74	-9.31
6	NH		5.96	-9.29	21	NH		6.36	-9.09
7	NH		5.72	-8.70	22	NH		7.24	-9.75
8	NH		5.60	-9.51	23	CH ₂		4.30	-7.74
9	NH		5.57	-10.27	24	CH ₂		5.61	-9.94
10	NH		5.36	-9.10	25	CH ₂		6.43	-9.68
11	NH		5.27	-7.59	26	CH ₂		7.24	-9.72
12	NH		4.82	-7.55	27	CH ₂		6.41	-9.32
13	NH		4.65	-8.55	28	CH ₂		7.55	-10.20
14	NH		3.98	-8.85	29	CH ₂		7.85	-10.18
15	NH		6.92	-9.55					

Table 2. Structures, HIV-1 RT inhibitory activity and AutoDock binding free energies of compounds in the test set.

									
Comp.	L	Ar	-LogIC ₅₀	ΔG (kcal/mol)	Comp.	L	Ar	-LogIC ₅₀	ΔG (kcal/mol)
30	NH		6.68	-8.83	36	NH		6.47	-9.40
31	NH		5.63	-9.05	37	NH		5.71	-9.47
32	NH		5.12	-8.97	38	CH ₂		5.08	-10.00
33	NH		4.49	-8.88	39	CH ₂		3.59	-7.90
34	NH		5.78	-9.06	40	CH ₂		4.87	-9.22
35	NH		7.26	-9.50					

structurally optimized using Gasteiger-Hückel partial charges and the Tripos force field. During minimization, atoms within 6 Å from the ligand were free to move (other atoms were fixed).

3D-QSAR studies

CoMFA and CoMSIA studies were performed based on the conformational alignment predicted from the molecular docking. Pyridinone derivatives with partial Gasteiger-Hückel charges or partial atomic charges based on the AM1 semiempirical molecular orbital method [47] implemented in Sybyl were used.

CoMFA. A 3D cubic lattice with grid spacing of 2 or 1 Å and extending 4 Å units beyond the aligned molecules in all directions was created. Steric and electrostatic interactions were calculated with the Tripos force field using a sp³ carbon probe atom with a charge of +1.0 with a distance-dependent dielectric at each lattice point. CoMFA descriptor fields were also calculated with a sp³ oxygen with -1.0 charge and a hydrogen atom with +1.0 charge as probe atoms. The minimum-sigma (column filtering) was set to 2.0 kcal/mol to improve the signal-to-noise ratio by

omitting those lattice points whose energy variation was below this threshold. A cutoff of 30 kcal/mol was adopted. The CoMFA steric and electrostatic fields generated were scaled by the CoMFA-STD method in Sybyl.

The CoMFA steric and electrostatic fields were used as independent variables and -logIC₅₀ values were used as dependent variables in the partial least squares (PLS) regression analyses to derive CoMFA models. The overall predictive ability of the analysis was evaluated first by leave-one-out (LOO) cross-validation. The cross-validated coefficient q^2 was calculated according to the following equation:

$$q^2 = (\text{SSY} - \text{PRESS})/\text{SSY}$$

SSY stands for the variance of the biological activities around the mean value, and PRESS is the prediction error sum of the squares, derived from the LOO method. The uncertainty of the prediction is defined as

$$\text{SPRESS} = [\text{PRESS}/(n - k - 1)]^{1/2}$$

where k is the number of variables in the model and n is the number of compounds used in the study. The number of components (noc) corresponding to the

lowest PRESS value was used for deriving the final PLS regression models. The conventional correlation coefficient r^2 was also computed as well as the conventional correlation coefficient for the prediction of compounds in the test set r^2_{pred} .

CoMSIA. The same grids constructed for the CoMFA fields calculation were used for CoMSIA fields calculation. The steric, electrostatic, hydrophobic, H-bond acceptor and H-bond donor similarity indices descriptors were calculated using a sp^3 carbon probe atom with a charge of +1.0 and a radius of 1.0 Å. The minimum-sigma was set to 2.0 kcal/mol. CoMSIA similarity indices (A_F) for a molecule j with atoms i at a grid point q are calculated by the following equation:

$$A_{F,k}^q(j) = -\sum \omega_{\text{probe},k} \omega_{ik} e^{-\alpha r_{iq}^2}$$

where q is the grid point for molecule j ; ω_{ik} the actual value of physicochemical property k of atom i ; $\omega_{\text{probe},k}$ indicates probe atom with charge +1, radius 1.0 Å, hydrophobicity +1, H-bond donor and acceptor property +1; α is the attenuation factor; r_{iq} is the mutual distance between probe atom at grid point q and atom i of the test molecule. Here, steric indices are related to the third power of the atomic radii, electrostatic descriptors are derived from atom-based parameters [48], and H-bond donor and acceptor indices are obtained by a rule-based method based on experimental results [49]. The default value of 0.3 was used as the attenuation factor for the Gaussian-type distance r_{iq} . The statistical evaluation for the CoMSIA analyses was performed in the same way as described for CoMFA.

Results and discussion

Docking

Before docking the pyridinone derivatives into the NNRTI binding site, the docking protocol was validated. Nevirapine was removed from the active site and docked back into the binding pocket. The root mean square deviation (RMSD) between the predicted conformation and the observed X-ray crystallographic conformation of nevirapine was 0.70 Å (Figure 2). Only one cluster was obtained with a mean docking energy of −9.66 kcal/mol. The top ranked binding conformation showed a docking energy of −9.67 kcal/mol and a free energy of binding of

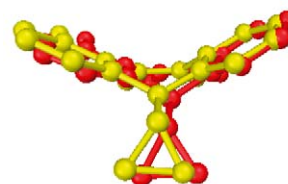


Figure 2. Comparison between the binding position of nevirapine found within the crystal structure (yellow) and the conformation predicted by AutoDock (red).

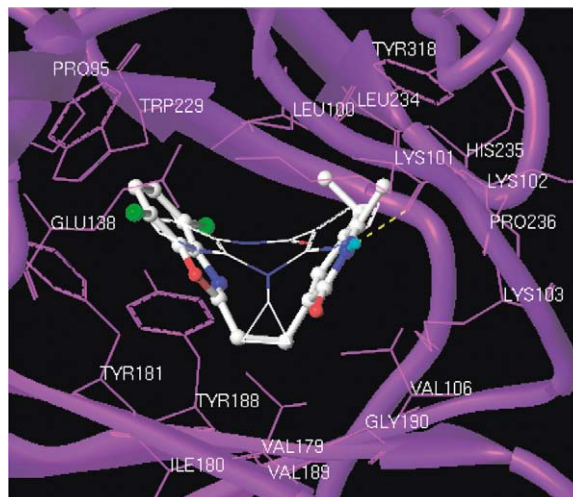


Figure 3. Optimized RT-29 complex. The hydrogen bond is displayed as yellow dashes. Amino acids within 5 Å of the benzoxazol and pyridinone rings are labeled. Nevirapine is displayed for comparison. Hydrogens are omitted for clarity except the polar hydrogen of the pyridinone ring.

−9.49 kcal/mol. These results indicated that the parameters used for AutoDock successfully reproduced the X-ray structure.

AutoDock found two possible binding modes for several pyridinone derivatives. The docked complexes of pyridinones-RT were selected according to the criteria of the most populated cluster combined with geometrical matching quality. In several cases the selected conformation corresponded to the lowest energy binding energy. According to this criterion all compounds adopt a butterfly-like conformation [50] into the NNRTI binding pocket and have the same orientation as nevirapine. The two aromatic rings ('wings') of the pyridinone derivatives may be roughly overlapped with the aromatic rings of nevirapine. The amino acid residues that interact with most of the docked pyridinone derivatives in this study were Pro95, Leu100, Lys101, Lys103, Tyr181, Tyr188 and Tyr318 of the p66 subunit (Figure 3). The corres-

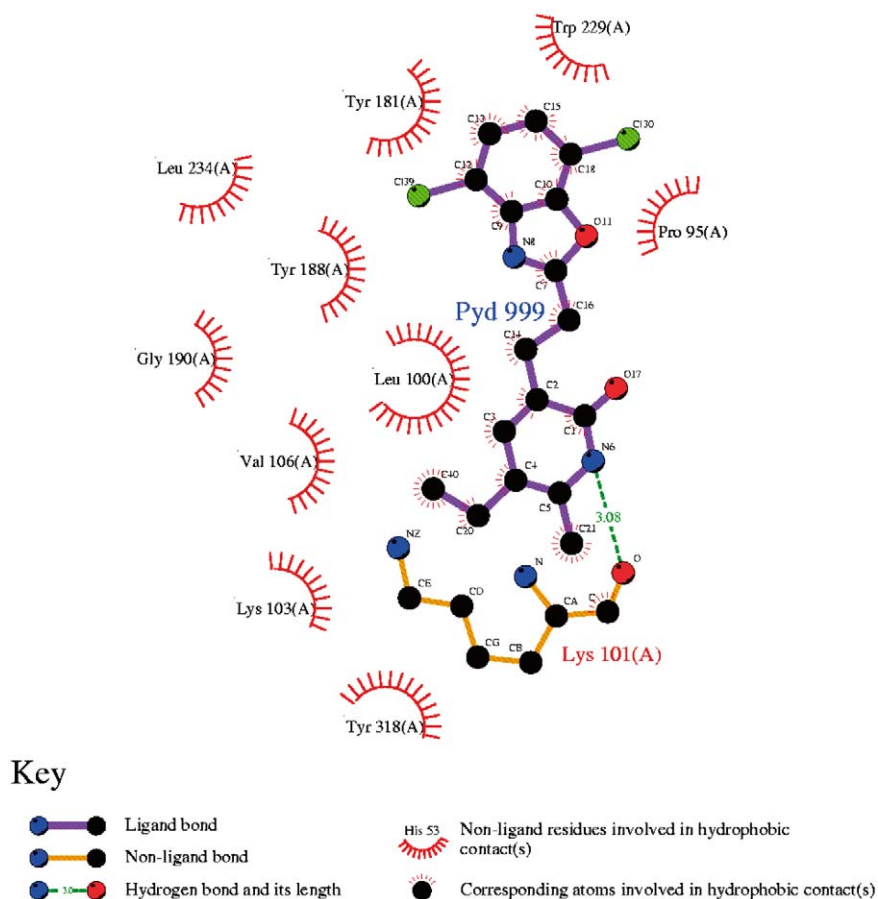


Figure 4. Two-dimensional representation of the main interactions of **29** with RT. The image was generated with the LIGPLOT program [51].

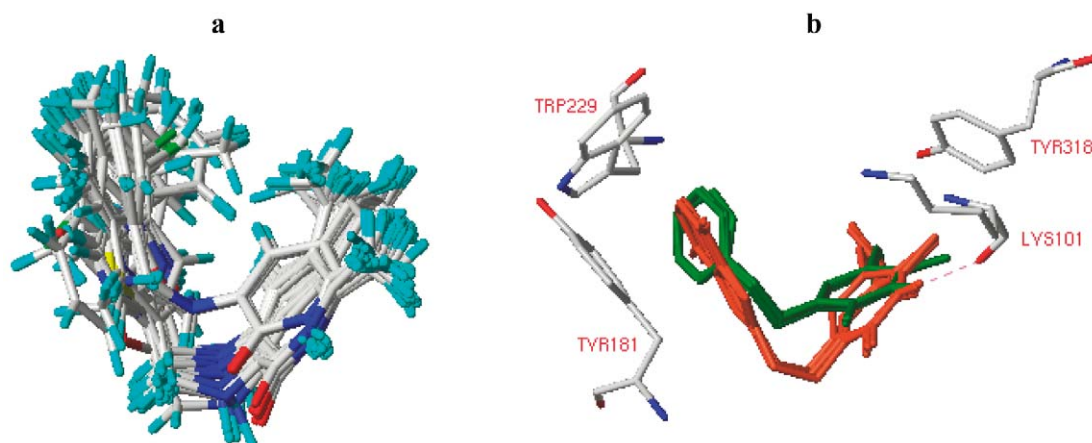


Figure 5. (a) Probable binding conformations of the pyridinone derivatives predicted by AutoDock and their alignment in the NNRTI binding site. (b) Comparison of the binding conformations of compounds **18**, **19**, **28** and **29** (orange) with **11**, **12**, **23** and **39** (green) in the binding site. The positions of Tyr181, Trp229, Tyr318 and Lys101 are displayed for reference. The hydrogen bond is displayed as magenta dashes. Hydrogens are omitted for clarity except for the polar hydrogen of the pyridinone ring.

ponding 2D interactions model for the most active compound is shown in Figure 4.

The molecular superposition of the binding conformations of the pyridinone derivatives extracted from the optimized inhibitor-RT complexes is shown in Figure 5a. All pyridinone derivatives have a common binding mode with a good overlapping of the pyridinone rings ('wing 1'). All docked compounds may form a hydrogen bond between the polar proton of the pyridinone ring and the main-chain carbonyl oxygen of Lys101 (Figures 3 and 4). A similar hydrogen bond to the main-chain carbonyl oxygen of Lys101 is observed for other NNRTIs [4b–d, g–i, k, l]. However, the 'wing 2' (the 'Ar' substituent in Tables 1 and 2) may adopt a different orientation depending on the chemical structure of the aromatic system (Figure 5b).

In a recent conformational analysis performed for pyridinone derivatives with different 'Ar' substituents [50], several minimum energy conformers were obtained for each pyridinone studied. The MMFF94 force field was used. Additional calculations based on the density functional theory were performed. The study revealed that the rotational barrier of the single bonds that connect the aromatic rings is small and that there is a marked preference for a butterfly-like conformation. We reached similar conclusions in a conformational analysis performed for compound **19** with Monte Carlo simulations and systematic search using molecular mechanics and semi-empirical methods (data not shown). For example, using semi-empirical calculations we observed that the highest rotational barrier of the benzoxazol ring is less than 1 kcal/mol. However, as part of the previous docking studies we conducted with pyridinone derivatives [34] starting from different minimum energy conformers, we observed that AutoDock predicts the same docked conformation regardless of the starting conformation. This indicates that AutoDock performs an efficient conformational search inside the binding pocket and suggests that the particular conformation predicted for each 'wing 2' is due to the specific interactions with the amino acids of the binding pocket.

Interestingly, the most active compounds have a benzoxazol ring. This two-ring system is close to Tyr181 (Figure 3). The parallel positions of the benzoxazol ring and the aromatic ring of Tyr181 suggest that they may be forming π -stacking interactions [52] and thus stabilizing the complex. Similar stabilizing interactions may occur for other pyridinone derivatives with a two-ring aromatic system in wing 2.

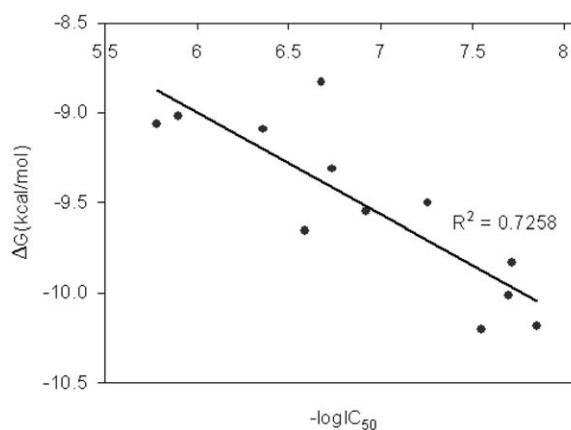


Figure 6. Plot of experimental activities vs. binding free energies (ΔG , $T=298.15$ K) for compounds with close structural similarity (**15–21**, **28**, **29**, **30**, **34**, **35**).

Compounds **11**, **12**, **23** and **39**, which have only one ring in the wing 2, adopt a docked position and conformation that is slightly different from the other pyridinone derivatives; the linker between the two wings is displaced upwards relative to the linker of the other pyridinone analogues (Figure 5b). Moreover, despite the fact that the wing 2 is close to Tyr181, the non-parallel positions of the phenyl group of Tyr181 and the wing 2 suggest weaker interactions between these systems (Figure 5b) [52]. This explains, at least in part, the low biological activity and the calculated high binding free energy of these compounds (Tables 1 and 2). Similarly, the low activity and the high binding free energy of **13** may be explained by the lack of contacts with Tyr181.

The predicted binding free energies of the pyridinone derivatives binding to RT are also listed in Tables 1 and 2. In general, the binding free energy calculated by AutoDock correlated well with the biological activity ($-\log IC_{50}$); compounds with the highest activities showed the lowest free energies. This suggests that the binding models for the pyridinone derivatives with RT are reasonable. A quantitative correlation between the binding free energy and the biological activity was better for structurally similar compounds, i.e., all compounds with a benzoxazol ring (Figure 6). All these compounds adopt a very similar binding mode.

3D-QSAR models

PLS results for the CoMFA and CoMSIA studies are summarized in Table 3. Figure 7 shows the prediction curves obtained with the CoMFA and CoMSIA mod-

Table 3. CoMFA and CoMSIA PLS statistics.^a

Charges	Step size	PLS statistics	29 Compds. model		28 Compds. model	
			CoMFA	CoMSIA	CoMFA	CoMSIA
AM1	2 Å	q^2	0.656	0.643	0.706	0.722
		PRESS	0.639	0.651	0.603	0.586
		Noc	4	4	4	4
		r^2	0.943	0.926	0.954	0.943
		S	0.259	0.295	0.239	0.266
		F	100.055	75.566	119.076	94.725
		r^2_{pred}	0.688	0.785	0.720	0.759
		Field contribution				
		Steric	0.608	0.121	0.600	0.122
		Electrostatic	0.392	0.421	0.400	0.434
		Hydrophobic		0.457		0.445
	1 Å	q^2	0.613	0.643	0.650	0.723
		PRESS	0.664	0.651	0.644	0.585
		Noc	3	4	3	4
		r^2	0.934	0.932	0.947	0.946
		S	0.275	0.284	0.251	0.259
		F	117.468	82.484	142.534	100.113
		r^2_{pred}	0.693	0.778	0.731	0.750
		Field contribution				
		Steric	0.563	0.121	0.559	0.121
		Electrostatic	0.437	0.426	0.441	0.434
		Hydrophobic		0.456		0.445
Gasteiger-Hückel	2 Å	q^2	0.558	0.569	0.627	0.621
		PRESS	0.710	0.715	0.694	0.685
		Noc	3	4	5	4
		r^2	0.920	0.934	0.955	0.941
		S	0.303	0.280	0.241	0.269
		F	95.341	84.812	93.199	92.289
		r^2_{pred}	0.771	0.729	0.715	0.780
		Field contribution				
		Steric	0.582	0.099	0.590	0.102
		Electrostatic	0.418	0.498	0.410	0.505
		Hydrophobic		0.403		0.393

^aDefault sp³ carbon as probe atom.

els. In Table 4 are presented the residual values from the prediction of the activity values of the test set.

To further test the stability and robustness of the 3D-QSAR models, the activities of compounds in the training set were shuffled 10 times. The q^2 of the models derived from these so-called random datasets were compared to those derived with the actual activities. The average q^2 after scrambling the biological data are presented in Table 5. These results indicate the stability and robustness in the CoMFA and CoMSIA models.

CoMFA. PLS analysis using AM1 charges and default parameters resulted in a CoMFA model with a good q^2 value of 0.656 and a r^2_{pred} value of 0.688. Omission of compound **3**, which was an outlier in this analysis, resulted in an increase in the q^2 value to 0.706 and in the r^2_{pred} value to 0.720 for the remaining 28 compounds. The outlier status of compound **3** cannot be successfully explained by the present results.

The effect of the grid spacing was investigated. Reducing the lattice step size from 2 to 1 Å reduced the q^2 from 0.656 to 0.613 for the model with all 29 com-

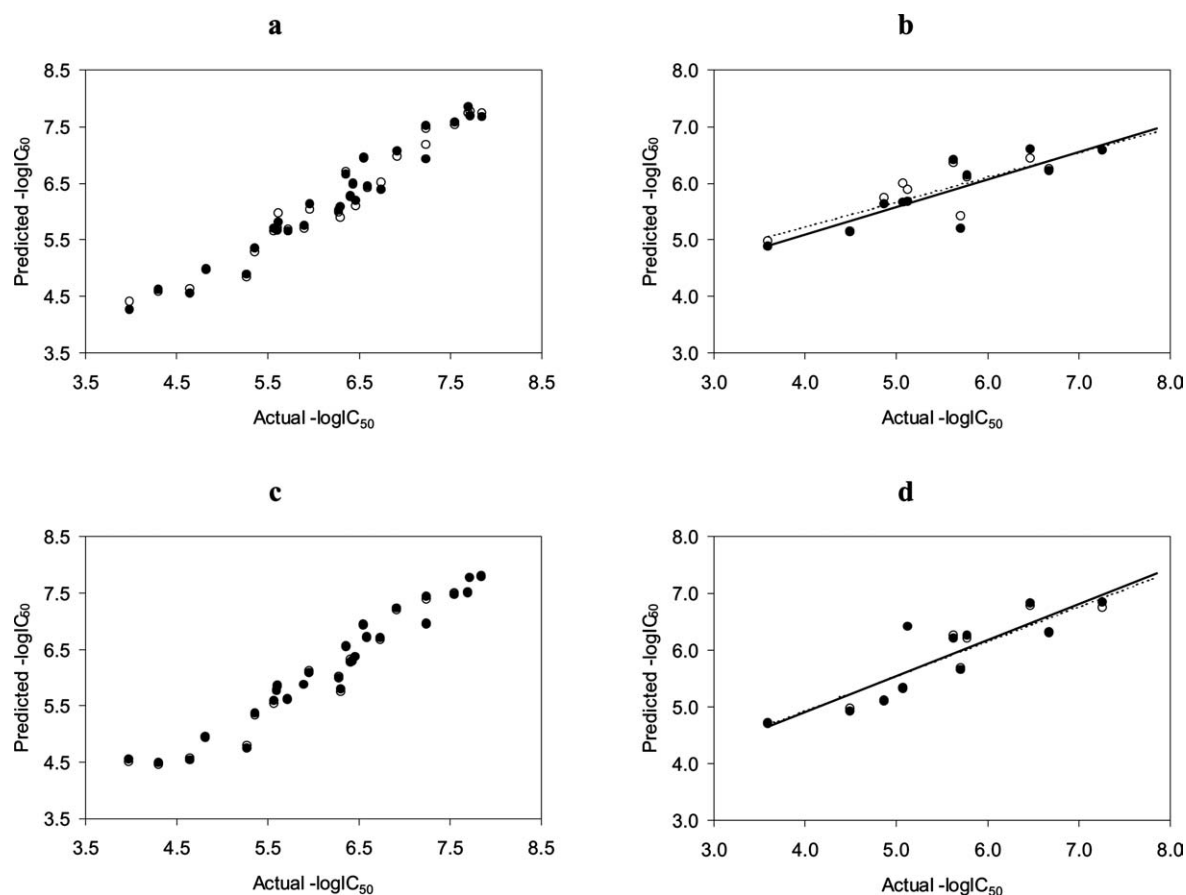


Figure 7. Predictions for the training and test sets with CoMFA and CoMSIA 28 compounds models. Predictions by the 2 Å model are in filled circles and solid lines, while predictions by the 1 Å model are in open circles and broken lines. The fitted curves for CoMFA models for the training and test sets are in panels a and b, respectively. The corresponding curves for the CoMSIA models are shown in panels c and d, respectively.

Table 4. Residuals of the predictions of the test set by the CoMFA and CoMSIA models.^a

Comp.	$-\log IC_{50}$	Residuals			
		CoMFA 2 Å	CoMFA 1 Å	CoMSIA 2 Å	CoMSIA 1 Å
30	6.68	0.462	0.429	0.360	0.376
32	5.63	-0.772	-0.736	-0.583	-0.628
33	5.12	-0.563	-0.758	-1.300	-1.300
34	4.49	-0.667	-0.646	-0.429	-0.474
35	5.78	-0.362	-0.318	-0.467	-0.424
36	7.26	0.671	0.674	0.424	0.511
37	6.47	-0.136	0.036	-0.348	-0.302
38	5.71	0.514	0.287	0.061	0.035
39	5.08	-0.576	-0.910	-0.258	-0.233
40	3.59	-1.283	-1.390	-1.128	-1.101
41	4.87	-0.752	-0.867	-0.228	-0.235

^a28 compounds models.

pounds and from 0.706 to 0.650 for the model with 28 compounds.

The predictive performance of the 28 compounds models is shown in Figure 7. The 2 Å model with 28 compounds was the best CoMFA model derived, showing a high predictive performance for the training ($q^2 = 0.706$) and test sets ($r^2_{pred} = 0.720$). However, the 1 Å model with 28 compounds showed the highest predictability for the test set with a r^2_{pred} value of 0.731, despite the lower q^2 value compared to the corresponding 2 Å model. Similarly, the 1 Å model with all compounds showed a higher r^2_{pred} than the corresponding 2 Å model with all compounds, despite its lower q^2 . This means that a higher q^2 value does not necessarily make a model more predictive with reference to an external test set, as previously pointed out in other 3D-QSAR studies [53].

In the 2 Å models with 29 and 28 compounds, the contribution of the steric interactions was 60.8 and 60.0%, respectively. In the 1 Å models the steric contribution was close to 56%. Interesting to note, a larger contribution of the steric interactions over the electrostatic interactions in CoMFA studies has been observed for other NNRTIs [27–29]. Furthermore, in some of these CoMFA analyses the contribution of the steric interactions is also around 60% [28, 29].

In all cases studied, the models derived with AM1 charges showed higher q^2 than those models obtained with Gasteiger-Hückel charges. However, models obtained with Gasteiger-Hückel charges showed a good predictability for the test set (Table 3). Concerning the variation of the probe atom, all models derived with a sp^3 carbon probe atom outperformed models obtained with a sp^3 oxygen and hydrogen as probe atoms (data not shown).

The PLS stdev* coefficient contour maps for the best CoMFA model are shown in Figure 8. To aid in visualization, compound **29** is displayed in the maps. Residues within 5 Å around the inhibitor were merged into the figure. Green regions indicate areas where steric bulk is predicted to enhance biological activity, whereas yellow regions indicate areas where steric bulk is detrimental to biological activity. There is a green contour close to the wing 2 of pyridinone derivatives which is also close to the position of Tyr181. This suggests a favorable interaction between the two systems. This observation further supports the discussion above that the interaction between the aromatic rings of the pyridinone derivatives and Tyr181 may be stabilizing the complex. According to the exper-

imental results for **29** and other potent pyridinone derivatives [8, 16], the mutation of Tyr181 to Cys seems to eliminate stabilizing contacts between the aromatic ring of tyrosine and the bound inhibitor, reducing the binding affinity.

A second favorable steric interaction is also close to the wing 2 and close to the position of the amino acids Tyr188 and Leu234 (Figure 8a). This contour agrees with the docked positions of molecules **17**, **20**, **21**, **35**, and **36** where the substituent at the benzoxazol or benzofuran ring is making contacts with these amino acids. The substituent at position 4 of the benzoxazol ring of compounds **18**, **19**, **28** and **29**, which are very potent pyridinone derivatives, also makes contacts with Tyr188 and Leu234. Interestingly, the second green contour is very close to the benzene ring of compounds **27** and **31**. These compounds with a medium-to-low activity do not make contacts with Tyr181 but with Tyr188. It seems that the interactions with Tyr188 make them not as inactive as expected from the lack of interactions with Tyr181.

These observations agree with the experimental data that mutation of Tyr188 is also responsible for the loss of activity of pyridinone derivatives [15, 16], although to a lesser extent when the mutation Tyr181Cys occurs. Indeed, the amino acids Tyr181 and Tyr188 are very important in the RT inhibition by NNRTIs. The loss of aromatic ring stacking interactions with Tyr181 and Tyr188 is thought to be responsible for the lack of activity of several so-called first generation NNRTIs against RT containing mutations of these amino acids [54]. These observations support the approach to modify the wing 2 of pyridinone derivatives to overcome the problem of mutations at Tyr181 is Tyr188 [34]. Examples of these modified pyridinone derivatives are the hybrid compounds pyridinone-EBPU and pyridinone-efavirenz in Figure 1 and the recently designed molecules by our group [34].

In Figure 8a there is a prominent yellow contour close to the wing 2 and the linker, suggesting steric restriction in this region. The side chains of Lys101 and Val179 are close to this region.

In Figure 8b are represented the electrostatic contributions as contour plots. Red contours illustrate areas where electronegative groups are predicted to favor activity and blue contours illustrate areas where electronegative groups are detrimental to biological activity. A large red electrostatic contour region close to the wing 2 of pyridinone derivatives indicates that high negative charges in this area enhance the affinity. These results are confirmed by the docked position of

Table 5. Average q^2 after scrambling the biological data.

Step size	29 Compds.		28 Compds.	
	CoMFA	CoMSIA	CoMFA	CoMSIA
2 Å	−0.144	−0.288	−0.157	−0.295
1 Å	−0.211	−0.286	−0.212	−0.293

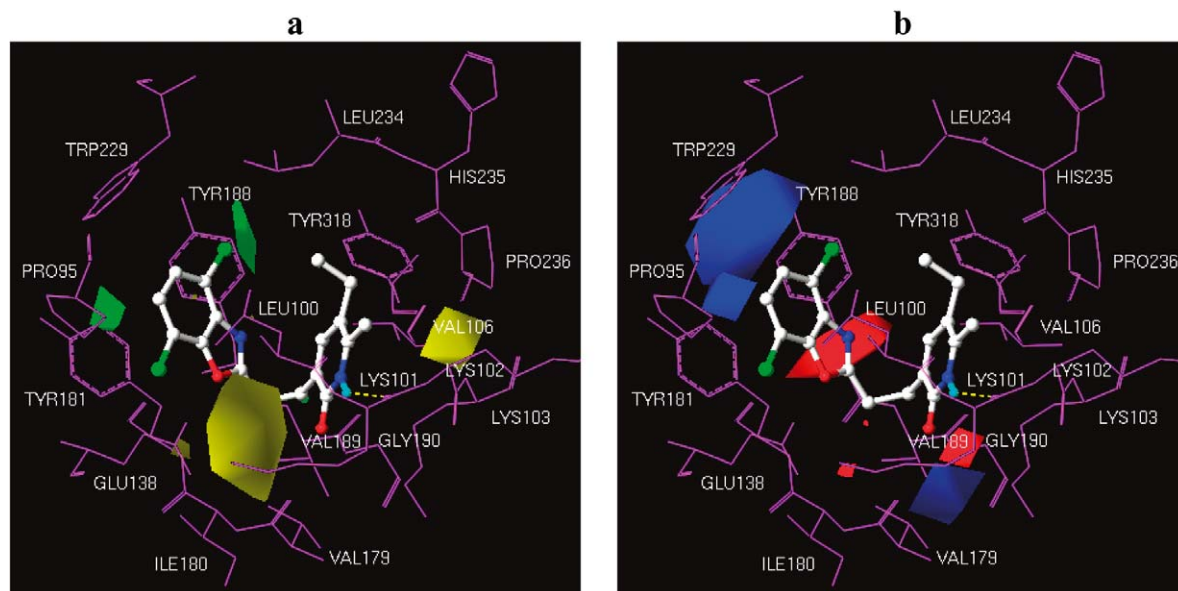


Figure 8. Stdev*coeff contour maps of best CoMFA model. Compound **29** and amino acids within 5 Å around the inhibitor are shown for clarity. (a) Steric contour maps. Sterically favored areas (contribution level of 80%) in green. Sterically unfavored areas (contribution level of 20%) in yellow. (b) Electrostatic contour maps. Negative-charge-favored areas (contribution level of 20%) in red. Negative-charge-unfavored areas (contribution level of 80%) in blue. The residues are in sticks and the inhibitor is in balls and sticks. The hydrogen bond is displayed as yellow dashes.

the wing 2 of molecules **2**, **4**, **5**, **10**, **18**, **19**, **22**, **24**, **25**, **28**, **29** and **36**. In all these cases, an atom with a high negative charge is oriented toward this region. This red contour explains the electrostatic contribution to the high activity of compounds **18**, **28** and **29**. There is a prominent blue contour close to the position of Trp229. The very low activity of compounds **14**, **33**, and **40** may be well explained by the presence of a nitrogen atom with a negative charge close to this contour. Similarly, a second but less prominent blue contour close to Pro95 explains the low activity of compound **7** that has a nitrogen atom with a negative charge close to this region.

CoMSIA. In the present study, we obtained better PLS statistics and predictive performance on the test set with the CoMSIA models than with the CoMFA models (Table 3). Using AM1 charges, default Sybyl

CoMSIA parameters and all compounds in the training set resulted in a model with a q^2 value of 0.643 and a r^2_{pred} value of 0.785 (as compared to a q^2 value of 0.656 and a r^2_{pred} value of 0.688 for CoMFA). However, elimination of the same outlier, compound **3**, brought the q^2 value up to 0.722 and the r^2_{pred} value to 0.759 (as compared to a q^2 value of 0.706 and a r^2_{pred} value of 0.720 for CoMFA). Reducing the grid spacing from 2 to 1 Å resulted in CoMFA PLS models with almost the same q^2 values (Table 3). However, the performance in predicting the activities of the test set was slightly lower (although higher than the predictive performance of the corresponding CoMFA models) (Table 3). The 1 Å model with 28 compounds was the best CoMSIA model derived with a q^2 value of 0.723 and a r^2_{pred} value of 0.750 (compare with the best CoMFA model derived with a q^2

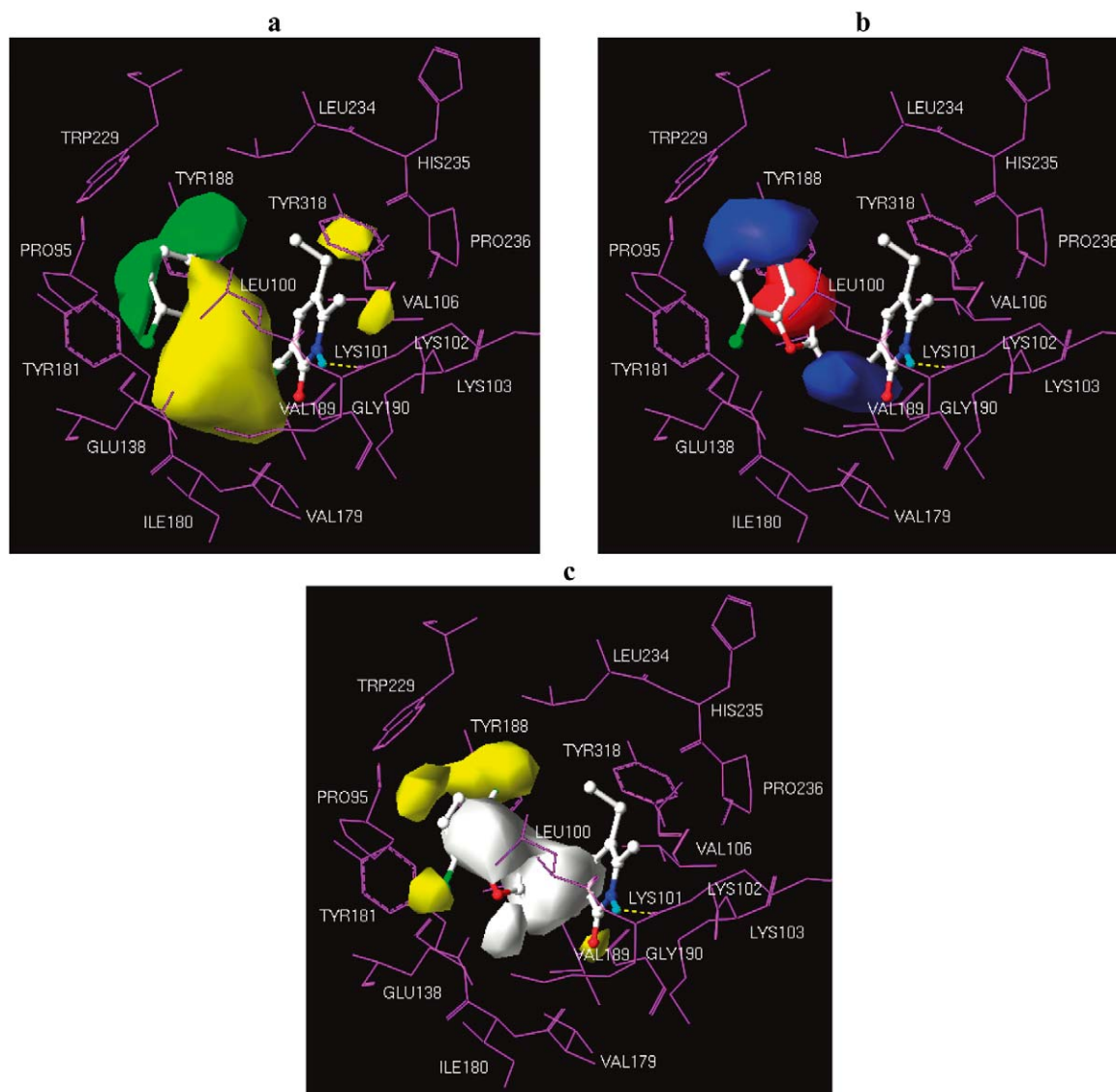


Figure 9. Stdev*coeff contour maps of best CoMSIA model. Compound **29** and amino acids within 5 Å around the inhibitor are shown for clarity. (a) Steric contour maps. (b) Electrostatic contour maps. The region colors have the same interpretation as those in Figures 8a and 8b, respectively. (c) Hydrophobic contour maps. Hydrophobically favored areas (contribution level of 80%) in yellow; hydrophobically unfavored areas (contribution level of 20%) in white. The residues, the inhibitor and the hydrogen bond are represented as in Figure 8.

value of 0.706 and a r^2_{pred} value of 0.720). The superior performance of CoMSIA relative to CoMFA, with this data set, may be attributed mainly to the contribution of the hydrophobic fields in the CoMSIA models. These types of descriptor fields are not available with standard CoMFA.

Similar strengths of steric and electrostatic fields were obtained in the best CoMFA and CoMSIA models (0.600 and 0.400, respectively, in CoMFA and 0.566 (S + H) and 0.434, respectively, in CoMSIA).

Similar to CoMFA, the models obtained with AM1 charges also showed higher q^2 than those models obtained with Gasteiger-Hückel charges. Models obtained with Gasteiger-Hückel charges showed a good predictability for the test set (Table 3).

The effect of the H-donor and H-acceptor CoMSIA fields on the PLS statistics was also investigated. Considering all five CoMSIA field and several field combinations did not improve the predictability of the obtained models (data not shown). This may be well

explained by the docking results. Only one hydrogen bond between pyridinone derivatives and the NNRTI binding site is predicted for all 29 compounds in the training set. Therefore, no differences in the binding affinities among the compounds should be expected from this hydrogen bond.

The PLS stdev* coefficient contour maps for the best CoMSIA model are shown in Figure 9. To aid in visualization, compound **29** is displayed in the maps. Residues within 5 Å around the inhibitor were merged into the figure. Color designation and interpretation for steric and electrostatic fields are the same as in the corresponding CoMFA contour maps.

Steric fields are similarly placed as those of the CoMFA model (Figure 8a). However, the two green CoMSIA contours close to the positions of Tyr181 and Tyr188 are more prominent than the corresponding contours obtained with CoMFA. This observation remarks the importance of the interactions between the pyridinone derivatives and Tyr181 and Tyr188 discussed previously.

The electrostatic fields of CoMSIA are generally in accordance with the field distribution of CoMFA maps (Figure 8b). It is interesting to note the additional blue contour surrounding the linker (see 'L' group in Tables 1 and 2) of several pyridinone derivatives, suggesting a preference for the ethylene linker over the amino methylene linker. This is confirmed by the higher activity and lower binding free energy of compounds **26**, **27** and **40** compared to their structurally related compounds **1**, **31** and **33**, respectively. The amino methylene group of **1**, **31** and **33**, where the nitrogen has a negative charge, is close to Tyr188 and Glu190, enabling negative interactions with the main-chain of these amino acids. However, compounds **23** and **39**, with an ethylene linker, are less active than their structurally related compounds **11** and **12**, respectively. This apparent exception may be explained, at least in part, because the blue contour does not surround the linker of these molecules. As discussed previously, these four molecules adopt a particular docked position such that the linker is above the linker of the other pyridinone derivatives (Figure 5b).

The hydrophobic analysis of CoMSIA could demonstrate more clearly the hydrophobic interactions between the pyridinone derivatives and RT. For the hydrophobic contour maps of CoMSIA, yellow contours indicate regions where increased hydrophobic interactions are associated with enhanced activity and white contours indicate regions where increased hydrophilic interactions are associated with enhanced activity. As

shown in Figure 9c, the yellow contours around the substituents at positions 4 and 7 of the benzoxazol ring of **29** indicate that these substituents interact with surrounding amino acids at the NNRTI binding site through hydrophobic interaction. Amino acids close to these contours are Tyr188 (close to the substituent at position 4), and the side chains of Pro95, Leu100 and Tyr181 (close to the substituent at position 7). This observation is in agreement with the SAR and 2D-QSAR studies for pyridinone derivatives with a benzoxazol ring. In these studies it was concluded that compounds di-substituted with methyl or chlorine groups at the positions 4 and 7 of the benzoxazol ring are more active than the corresponding mono- or unsubstituted compounds [6, 11, 12]. An example of these di-substituted potent inhibitors is compound **29**.

The present 3D-QSAR models did not explain the experimentally observed loss of activity due to the Lys103Asn mutation [8, 13–15]. Since all derivatives studied have the same pyridinone ring, no significant contours around this ring may be interpreted. However, from the docking studies it is observed that the pyridinone ring makes important contacts with Lys103 (Figures 3 and 4) [34].

Conclusions

We predicted the binding conformations of 40 pyridinone derivatives into the NNRTI binding pocket using AutoDock. The molecules adopt a butterfly-like conformation and most of them have a common binding mode which is similar to the binding conformation of nevirapine. The binding free energies calculated by this method correlated well with the reported inhibitory activities against RT. The correlation was better for most similar compounds. Starting from the docked positions of the pyridinone derivatives, we performed 3D-QSAR analyses. Robust CoMFA and CoMSIA models were obtained with a high predictability performance for the training and test sets. CoMSIA models performed slightly better than CoMFA models. The good 3D-QSAR models obtained further validated the reasonableness of the docking predictions by AutoDock. According to the 3D-QSAR models, steric, electrostatic and hydrophobic interactions occur between the inhibitors and the NNRTI binding pocket. Important interactions with the amino acids Tyr181 and Tyr188 were predicted which further explained the loss of activity of pyridinones against RT containing mutations. These interactions also help to rationalize

at the molecular level, at least in part, the design of hybrid pyridinone molecules, and support the approach to modify the benzoxazol ring of potent pyridinone derivatives to overcome the problem of Tyr181Cys and Tyr188Cys mutations. The 3D-QSAR models derived will be useful for the rational design of pyridinone derivatives active against RT containing mutations.

Acknowledgements

The authors are very grateful to Dr. A. Olson and his colleagues at the Scripps Research Institute for providing AutoDock and to Dr. Roman Laskowski for providing LIGPLOT. J.L. Medina-Franco is grateful to CONACyT and DGAPA, UNAM, for the Ph. D. thesis scholarships. We also would like to acknowledge CONACyT for financing project G-34851-M.

References

- De Clercq, E., *Biochim. Biophys. Acta*, 1587 (2002) 258.
- De Clercq, E., *Antivir. Res.*, 38 (1998) 153.
- Esnouf, R., Ren, J., Ross, C., Jones, Y., Stammers, D. and Stuart, D., *Nat. Struct. Biol.*, 2 (1995) 303.
- (a) Ren, J., Esnouf, R., Garman, E., Somers, D., Ross, C., Kirby, I., Keeling, J., Darby, G., Jones, Y., Stuart, D. and Stammers, D., *Nat. Struct. Biol.*, 2 (1995) 293. (b) Hopkins, A.L., Ren, J., Esnouf, R.M., Willcox, B.E., Jones, E.Y., Ross, C., Miyasaka, T., Walker, R.T., Tanaka, H., Stammers, D.K. and Stuart, D.I., *J. Med. Chem.*, 39 (1996) 1589. (c) Ren, J., Esnouf, R., Hopkins, A., Ross, C., Jones, Y., Stammers, D. and Stuart, D., *Structure*, 3 (1995) 915. (d) Ren, J., Milton, J., Weaver, K. L., Short, S.A., Stuart, D.I. and Stammers, D.K., *Structure*, 8 (2000) 1089. (e) Ren, J., Nichols, C., Bird, L.E., Fujiwara, T., Sugimoto, H., Stuart, D.I. and Stammers, D.K., *J. Biol. Chem.*, 275 (2000) 14316. (f) Esnouf, R.M., Ren, J., Hopkins, A. L., Ross, C.K., Jones, E.Y., Stammers, D.K. and Stuart, D.I., *Proc. Natl. Acad. Sci. USA*, 94 (1997) 3984. (g) Ren, J., Diprose, J., Warren, J., Esnouf, R.M., Bird, L.E., Ikemizu, S., Slater, M., Milton, J., Balzarini, J., Stuart, D.I. and Stammers, D.K., *J. Biol. Chem.*, 275 (2000) 5633. (h) Chan, J.H., Hong, J.S., Hunter III, R.N., Orr, G.F., Cowan, J.R., Sherman, D.B., Sparks, S.M., Reitter, B.E., Andrews III, C.W., Hazen, R.J., St Clair, M., Boone, L.R., Ferris, R.G., Creech, K.L., Roberts, G.B., Short, S.A., Weaver, K., Ott, R.J., Ren, J., Hopkins, A., Stuart, D.I. and Stammers, D.K., *J. Med. Chem.*, 44 (2001) 1866. (i) Hsiou, Y., Das, K., Ding, J., Clark Jr., A.D., Kleim, J.P., Rosner, M., Winkler, I., Riess, G., Hughes, S.H. and Arnold, E., *J. Mol. Biol.*, 284 (1998) 313. (j) Ren, J., Esnouf, R.M., Hopkins, A.L., Stuart, D.I. and Stammers, D.K., *J. Med. Chem.*, 42 (1999) 3845. (k) Ren, J., Esnouf, R.M., Hopkins, A.L., Warren, J., Balzarini, J., Stuart, D.I. and Stammers, D.K., *Biochemistry*, 37 (1998) 14394. (l) Hogberg, M., Sahlberg, C., Engelhardt, P., Noreen, R., Kangasmetsa, J., Johansson, N.G., Oberg, B., Vrang, L., Zhang, H., Sahlberg, B. L., Unge, T., Lovgren, S., Fridborg, K. and Backbro, K., *J. Med. Chem.*, 43 (2000) 304.
- Goldman, M.E., Nunberg, J.H., O'Brien, J.A., Quintero, J.C., Schleif, W.A., Freund, K.F., Gaul, S.L., Saari, W.S., Wai, J.S., Hoffman, J.M., Anderson, P.S., Hupe, D.J., Emini, E.A. and Stern, A.M., *Proc. Natl. Acad. Sci. USA*, 88 (1991) 6863.
- Garg, R., Gupta, S.P., Gao, H., Babu, M.S., Debnath, A.K. and Hansch, C., *Chem. Rev.*, 99 (1999) 3525.
- Gupta, S.P., In Jucker, E. (Ed.), *Progress in Drug Research*, Vol. 58, Birkhäuser Verlag, Basel, Switzerland, 2002, pp. 252–253.
- Nunberg, J.H., Schleif, W.A., Boots, E.J., O'Brien, J.A., Quintero, J.C., Hoffman, J.M., Emini, E.A. and Goldman, M.E., *J. Virol.*, 65 (1991) 4887.
- Saari, W.S., Hoffman, J.M., Wai, J.S., Fisher, T.E., Rooney, C.S., Smith, A.M., Thomas, C.M., Goldman, M.E., O'Brien, J.A., Nunberg, J.H., Quintero, J.C., Schleif, W.A., Emini, E.A., Stern, A.M. and Anderson, P.S., *J. Med. Chem.*, 34 (1991) 2922.
- Hoffman, J.M., Wai, J.S., Thomas, C.M., Levin, R.B., O'Brien, J.A. and Goldman, M.E., *J. Med. Chem.*, 35 (1992) 3784.
- Saari, W.S., Wai, J.S., Fisher, T.E., Thomas, C.M., Hoffman, J.M., Rooney, C.S., Smith, A.M., Jones, J.H., Bamberger, D.L., Goldman, M.E., O'Brien, J.A., Nunberg, J.H., Quintero, J.C., Schleif, W.A., Emini, E.A. and Anderson, P.S., *J. Med. Chem.*, 35 (1992) 3792.
- Hoffman, J.M., Smith, A.M., Rooney, C.S., Fisher, T.E., Wai, J.S., Thomas, C.M., Bamberger, D., Barnes, J.L., Williams, T. M., Jones, J.H., Olson, B.D., O'Brien, J.A., Goldman, M.E., Nunberg, J.H., Quintero, J.C., Schleif, W.A., Emini, E.A. and Anderson, P.S., *J. Med. Chem.*, 36 (1993) 953.
- Davey, R.T., Dewar, R.L., Reed, G.F., Vasudevachari, M.B., Polis, M.A., Kovacs, J.A., Fallon, J., Walker, R.E., Masur, H., Haneiwich, S.E., O'Neill, D.G., Decker, M.R., Metcalf, J.A., Deloria, M.A., Laskin, O.L., Salzman, N. and Lane, H.C., *Proc. Natl. Acad. Sci. USA*, 90 (1993) 5608.
- Saag, M.S., Emini, E.A., Laskin, O.L., Douglas, J., Lapidus, W.I., Schleif, W.A., Whitley, R.J., Hildebrand, C., Byrnes, V.W., Kappes, J.C., Anderson, K.W., Massari, F.E., Shaw, G.M. and L-697,661 Working Group, *N. Engl. J. Med.*, 329 (1993) 1065.
- Sardana, V.V., Emini, E.A., Gotlib, L., Graham, D.J., Lineberger, D.W., Long, W.J., Schlabach, A.J., Wolfgang, J.A. and Condra, J.H., *J. Biol. Chem.*, 267 (1992) 17526.
- Byrnes, V.W., Sardana, V.V., Schleif, W.A., Condra, J.H., Waterbury, J.A., Wolfgang, J.A., Long, W.J., Schneider, C.L., Schlabach, A.J., Wolanski, B.S., Graham, D.J., Gotlib, L., Rhodes, A., Titus, D.L., Roth, E., Blahy, O.M., Quintero, J. C., Staszewski, S. and Emini, E.A., *Antimicrob. Agents Chemother.*, 37 (1993) 1576.
- Jourdan, F., Renault, J., Fossey, C., Bureau, R., Ladurée, D., Robba, M., Aubertin, A.M. and Kirn, A., *Antivir. Chem. Chemother.*, 8 (1997) 161.
- Dollé, V., Fan, E., Nguyen, C. H., Aubertin, A.M., Kirn, A., Andreola, M.L., Jamieson, G., Tarrago-Litvak, L. and Bisagni, E., *J. Med. Chem.*, 38 (1995) 4679.
- Dollé, V., Nguyen, C. H., Legraverend, M., Aubertin, A.M., Kirn, A., Andreola, M.L., Ventura, M., Tarrago-Litvak, L. and Bisagni, E., *J. Med. Chem.*, 43 (2000) 3949.
- Corbett, J.W., Kresge, K.J., Pan, S., Cordova, B.C., Klabe, R. M., Rodgers, J.D. and Erickson-Viitanen, S.K., *Bioorg. Med. Chem. Lett.*, 11 (2001) 309.
- Pungpo, P., Hannongbua, S. and Wolschann, P., *Curr. Med. Chem.*, 10 (2003) 1661, and references therein.

22. Douali, L., Villemin, D. and Cherqaoui, D., *J. Chem. Inf. Comput. Sci.*, 43 (2003) 1200.
23. Cramer III, R.D., Patterson, D.E. and Bunce, J.D., *J. Am. Chem. Soc.*, 110 (1988) 5959.
24. Klebe, G., Abraham, U. and Mietzner, T., *J. Med. Chem.*, 37 (1994) 4130.
25. Kubinyi, H. (Ed.) *3D QSAR in Drug Design: Theory, Methods and Applications*, ESCOM, Leiden, The Netherlands, 1993.
26. Barreca, M.L., Carotti, A., Carrieri, A., Chimirri, A., Monforte, A.M., Calace, M.P. and Rao, A., *Bioorg. Med. Chem.*, 7 (1999) 2283.
27. Hannongbua, S., Pungpo, P., Limtrakul, J. and Wolschann, P., *J. Comput.-Aided Mol. Des.*, 13 (1999) 563.
28. Pungpo, P. and Hannongbua, S., *J. Mol. Graph. Mod.*, 18 (2000) 581.
29. Hannongbua, S., Nivesanond, K., Lawtrakul, L., Pungpo, P. and Wolschann, P., *J. Chem. Inf. Comput. Sci.*, 41 (2001) 848.
30. Chen, H.F., Yao, X.J., Li, Q., Yuan, S.G., Panaye, A., Doucet, J.P. and Fan, B.T., *SAR QSAR Environ. Res.*, 14 (2003) 455.
31. Titmuss, S.J., Keller, P.A. and Griffith, R., *Bioorg. Med. Chem.*, 7 (1999) 1163.
32. Zhou, Z., Madrid, M. and Madura, J.D., *Proteins*, 49 (2002) 529.
33. Kontoyianni, M., McClellan, L.M. and Sokol, G.S., *J. Med. Chem.*, 47 (2004) 558.
34. Medina-Franco, J.L., Rodríguez-Morales, S., Juárez-Gordiano, C., Hernández-Campos, A., Jiménez-Barbero, J. and Castillo, R., *Bioorg. Med. Chem.*, 2004 *submitted for publication*.
35. Lozano, J.J., Pastor, M., Cruciani, G., Gaedt, K., Centeno, N. B., Gago, F. and Sanz, F., *J. Comput.-Aided Mol. Des.*, 14 (2000) 341.
36. Sippl, W., Contreras, J.-M., Parrot, I., Rival, Y.M. and Wermuth, C.G., *J. Comput.-Aided Mol. Des.*, 15 (2001) 395.
37. Sippl, W., *J. Comput.-Aided Mol. Des.*, 16 (2002) 825.
38. Sippl, W., *Bioorg. Med. Chem.*, 10 (2002) 3741.
39. Morris, G.M., Goodsell, D.S., Halliday, R.S., Huey, R., Hart, W.E., Belew, R.K. and Olson, A.J., *J. Comput. Chem.*, 19 (1998) 1639.
40. Brookhaven Protein Data Bank. <http://www.rcsb.org>.
41. Sybyl 6.8, Tripos Associates, Inc., St. Louis, MO, USA.
42. Clark, M., Cramer III, R.D. and Van Opdenbosch, N., *J. Comput. Chem.*, 10 (1989) 982.
43. Streitwieser, A. (Ed.) *Molecular Orbital Theory for Organic Chemists*, Wiley, New York, 1961.
44. Weiner, S.J., Kollman, P.A., Case, D.A., Singh, U.C., Ghio, C., Alagona, G., Profeta, S. and Weiner, P., *J. Am. Chem. Soc.*, 106 (1984) 765.
45. Gasteiger, J. and Marsili, M., *Tetrahedron*, 36 (1980) 3219.
46. Mehler, E.L. and Solmajer, T., *Protein Eng.*, 4 (1991) 903.
47. Dewar, M.J.S., Zoebisch, E.G., Healy, E.F. and Stewart, J.J. P., *J. Am. Chem. Soc.*, 107 (1985) 3902.
48. Viswanadhan, V.N., Ghose, A.K., Revenkar, G.R. and Robins, R., *J. Chem. Inf. Comput. Sci.*, 29 (1989) 163.
49. Klebe, G., *J. Mol. Biol.*, 237 (1994) 212.
50. Parreira, R.L.T., Abrahão, O. and Galembeck, S.E., *Tetrahedron*, (2001) 3243.
51. Wallace, A.C., Laskowski, R.A. and Thornton, J.M., *Protein Eng.*, 8 (1995) 127.
52. McGaughey, G.B., Gagné, M. and Rappé, A., *J. Biol. Chem.*, 273 (1998) 15458.
53. Buolamwini, J.K. and Assefa, H., *J. Med. Chem.*, 45 (2002) 841.
54. Ren, J., Nichols, C., Bird, L., Chamberlain, P., Weaver, K., Short, S., Stuart, D.I. and Stammers, D. K., *J. Mol. Biol.*, 312 (2001) 795.